

Investigating the Copper Doping Effects on the Performance of CoO_x Based CH₃NH₃PbI₃ Perovskite Solar Cells

Pelin Kavak 

Yıldız Technical University, Faculty of Arts and Science, Department of Physics, İstanbul, Türkiye,
paydogan@yildiz.edu.tr, ror.org/0547yzj13

ARTICLE INFO

ABSTRACT

Keywords:

Cobalt oxide
Perovskite
Hole transport layer
Cu doping
MAPbI₃

Article History:

Received: 23.03.2025

Revised: 21.05.2025

Accepted: 30.05.2025

Online Available: 10.06.2025

Perovskite solar cells have garnered extensive focus in recent years owing to their unique characteristics and promising potential in photovoltaic applications. Hole transport layers (HTL) composed of metals are critical components for achieving stable performance in CH₃NH₃PbI₃ perovskite solar cells. This study demonstrates the effect of metal doping in the CoO_x HTL. A systematic investigation of photovoltaic performance was conducted using a fast and practical solution-based approach, incorporating Cu as a dopant. The structural and morphological properties were observed through surface roughness and electrical measurements. The Cu-doped CoO_x film exhibited improved photovoltaic performance compared to its undoped counterpart, with efficiency reaching 9.02% from 6.17%.

1. Introduction

Perovskite solar cells have been the focus of growing scientific attention over the past ten years due to their advantageous characteristics, such as cost-effectiveness, efficient charge carrier transport, high optical absorption coefficient, and low thermal fabrication [1-3]. These advantages, coupled with superior electron and hole mobility, have allowed perovskite solar cells to reach an outstanding power conversion efficiency (PCE) of 27% [4], making them a promising candidate for next-generation photovoltaic technologies. Perovskite structures are typically represented by the ABX₃ formula, in which A and B correspond to cations of different dimensions, while X is an anionic species.

In photovoltaic devices utilizing these compounds as the active layer, they exhibit notable photovoltaic conversion efficiency (PCE) [5]. Perovskite solar cells can be categorized into planar or mesoporous types based on their device architecture [6-8]. The planar structure can be further classified into two

configurations: conventional (n-i-p) and inverted (p-i-n), based on the arrangement of charge transport layers, where "p" represents the hole transport material and "n" denotes the electron transport material [9]. There are two primary fabrication routes for perovskite solar cells: vacuum deposition techniques [10-11] and solution-based techniques.

The solution-based techniques are further subdivided into three major approaches: one-step deposition [12-13], spray coating [14], and two-step deposition [15]. To achieve pinhole-free perovskite films with uniform grain morphology, evaporation-based methods are employed; however, these techniques require high vacuum systems. The one-step deposition strategy is classified into two approaches: Solvent annealing [16-17] and antisolvent washing [18]. Long-term stability remains a critical issue in perovskite solar cells, emphasizing the need for improved charge carrier transport and minimized trap density at grain boundaries [19]. The hole transport layer (HTL) is essential in perovskite solar cells, performing several key functions

critical for device performance. Initially, it acts as a barrier between the metal electrode and the electron transport layer (ETL), improving interfacial conductivity while suppressing electron-hole recombination. Secondly, the HTL enhances the device's internal quantum efficiency (IQE) by mitigating charge losses at the interfaces.

Lastly, it increases the back electrode's reflectivity, enabling a second pass of light through the absorber layer for improved light absorption [20]. In inverted perovskite solar cells (PSCs), various inorganic p-type semiconductors, such as NiO_x [21], MoO_x [22], V_2O_x [23], Cu_2O [24], and CoO_x [25], have been utilized as hole transport layers. Inorganic HTLs outperform other types of HTLs due to their ability to enhance device performance and enable cost-effective perovskite solar cell fabrication, while also offering enhanced charge transport properties, well-aligned energy levels, and inherent thermal and chemical stability. NiO_x -based PSCs have attracted considerable attention, as NiO_x serves as an effective hole transport material for inverted PSCs. Its wide band gap, deep valence band, strong chemical stability, and facile deposition techniques make it highly advantageous [26].

Originally reported by Shalan et al. [25] as an HTL for perovskite solar cells, CoO_x -based solar cells are drawing considerable interest due to their sustainability, eco-friendly nature, solution processability and low-cost production. To enhance their efficiency, various approaches, including doping and morphological modifications, have been explored [27]. Doping is an effective technique for tailoring the optical and electrical properties of semiconductors. A range of metals have been incorporated as dopants into inorganic metal oxides to alter their properties and improve their performance. [28-29]. The incorporation of Cu into the NiO_x structure significantly enhances charge transport and reduces interfacial recombination, resulting in notable efficiency and improved device stability in inverted perovskite solar cells [30]. Also, cobalt doping into NiO_x has significantly improved the electrical conductivity and hole transport capability of the hole transport layer [31]. The incorporation of Mn ions has altered

the electronic band structure, increasing charge carrier mobility and electrical conductivity, thereby making Mn-doped NiO_x a promising material for electronic and optoelectronic applications [32].

In this work; an extensive investigation of copper doping strategies for optimizing cobalt oxide HTLs in MAPbI_3 -based perovskite solar cells is provided. The deposition of cobalt oxide layers was carried out by using spin-coating method, followed by precise heat processing under regulated conditions. Importantly, the perovskite layer deposition and the overall deposition method were performed without the use of a glove box. Figure 1 illustrates the structural and energy level diagram of device.

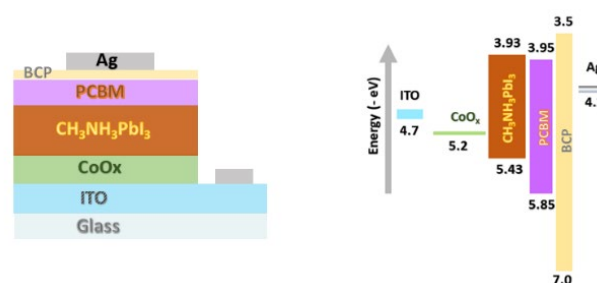


Figure 1. Structural and energy level scheme of device

2. Materials and Methods

2.1. Materials

The chemicals were applied directly as received, without any additional purification steps or modification including Methylammonium iodide (MAI) (>99.9 %, Ossila), Copper (II) acetate monohydrate ($\text{Cu}(\text{CO}_2\text{CH}_3)_2\text{H}_2\text{O}$) (99%, Sigma-Aldrich), Lead iodide (PbI_2) (99%, Sigma-Aldrich), diethanolamine (DEA) ($\text{C}_4\text{H}_{11}\text{NO}_2$) (99.5%, Sigma-Aldrich), [6]-phenyl-C61-butyric acid methyl ester (PCBM) (99%, Ossila), BCP (99.5 %, Ossila), Indium tin oxide coated substrates (ITO) (Labkon). Aluminum pellets were acquired from Kurt J. Lesker Company.

2.2. Fabrication of perovskite solar cells

ITO-coated glass substrates were divided into smaller pieces with dimensions of $1.5 \text{ cm} \times 1.5 \text{ cm}$ and rinsed in ultrasonic cleaner in succession

using deionized water, acetone and isopropanol for 30 minutes, respectively. UV-ozone was treated for 10 minutes prior to use to remove the organic residues, then they were moved to the spin coater. The precursor solutions for cobalt oxide were synthesized by dissolving 62.5 mg of cobalt (II) acetate tetrahydrate in 2.5 mL of ethanol at room temperature, followed by the addition of 12.5 μL of DEA to ensure the total dissolution of the cobalt salt. Copper (II) acetate monohydrate was introduced into the main precursor and mixed at room temperature for 4h to perform the incorporation process. Doped and pure CoO_x -based precursor solutions were spin-coated onto glass/indium thin oxide substrates at 2000 rpm for 45 s, and then thermally treated at 350 $^\circ\text{C}$ for 20 minutes in environmental air. Then, all coated substrates were allowed to reach room temperature for further perovskite deposition.

The MAPbI_3 perovskite precursors were synthesized by dissolving 111 mg of MAI and 322.5 mg PbI_2 with 0.5 ml GBL (γ -butyrolactone) at 50 $^\circ\text{C}$ for 24 hours to dissolve all precursors completely. The solution of perovskite was spin-cast by dripping 100 μl of toluene over the spinning layer at 5 seconds before the end of the procedure. Then, the perovskite films were thermally treated in ambient air at 100 $^\circ\text{C}$ for 15 minutes. The substrates were cooled to room temperature, and then, the PCBM layer was spin-coated at 2000 rpm for 20 seconds. The PCBM solution was prepared by dissolving 10 mg of PCBM in 500 μL of dichlorobenzene. The BCP solution prepared by dissolving 1mg/ml of BCP powder in ethanol was spin-coated at 4000 rpm for 20 seconds. In the end, ~ 110 nm Ag was thermally evaporated under a pressure of $\sim 10^{-6}$ Pa over the electron transfer layer to form the back contact. The entire sol-gel fabrication process was carried out in ambient air with a humidity level of 40%. Device fabrication steps were given in Figure 2.

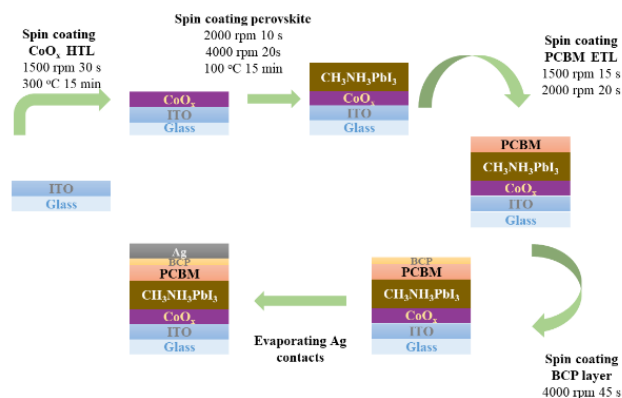


Figure 2. Solar cell fabrication steps

2.3. Device and film characterizations

Current density-voltage measurements were carried out by a digital source meter Keithley 2400 under AM 1.5G (100 mW/cm^2) illumination through an ABET solar simulator. Devices were measured at a scan rate of 0.25 V/s. All the measurements of the solar cells were carried out in a glove box at room temperature. X-ray diffraction (XRD) analysis of pure and Cu-doped MAPbI_3 perovskites was obtained using a PANalytical Empyrean Diffractometer to examine the crystal structure of the films. The atomic force microscopy (AFM) was carried out to determine the HTLs surface roughness using an AFM workshop with contact mode using silicon tips over a $5 \times 5 \mu\text{m}$ area.

The light absorption properties were performed in the spectral range of 400–1200 nm with a Perkin Elmer Lambda 35 UV/VIS. Field emission scanning electron microscopy (FESEM) (Thermo Scientific Apreo 2S) was utilized to investigate the morphological characteristics of perovskite films deposited on doped and undoped CoO_x layers.

3. Results and Discussion

To characterize the electrical conductivity variations induced by Cu doping in CoO_x , AFM measurements were employed, examining both undoped and Cu-doped CoO_x films on ITO substrates, as depicted in Figure 3. The roughness values for the pure and Cu-doped films were found to be 2.14 nm and 4.44 nm, respectively. Therefore, the roughness value shows a slight increase as the grain size grows with Cu doping [33].

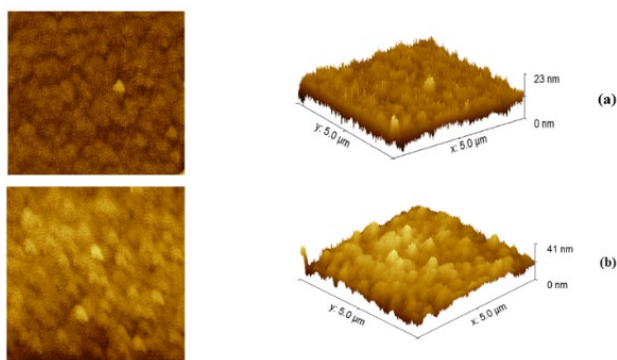


Figure 3. AFM images of (5 $\mu\text{m} \times 5 \mu\text{m}$) (a) undoped CoO_x and (b) Cu-doped CoO

Figure 4 illustrates the transmission spectra of the Cu-doped and pure CoO_x films on indium thin oxide substrates in the wavelength range of 400 to 1200 nm. The Cu-doped CoO_x film exhibits lower transmission in the visible region, which is attributed to the increased scattering effect caused by the rough surface morphology of the Cu-doped CoO_x hole transport layer [33].

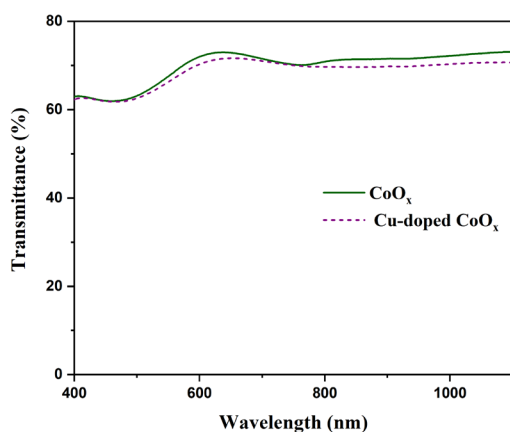


Figure 4. Transmission spectrum of undoped and Cu-doped CoO_x

The topographic structure of the perovskite thin films was performed by using field emission scanning electron microscopy (FE-SEM) to gain insight into the device's performance. Figure 5 presents FE-SEM pictures of MAPbI_3 surfaces coated on both CoO_x and Cu-doped CoO_x layers. The images demonstrate that perovskite growth on Cu-doped CoO_x was successfully realized, showing smaller grain sizes and a uniform distribution of grains without the presence of pinholes. A decrease in grain size led to lower exciton recombination losses, resulting in improved photovoltaic efficiency of the device

[34]. In contrast, the formation of pinholes on the perovskite surface of undoped CoO_x has been observed, that negatively impact the overall device efficiency.

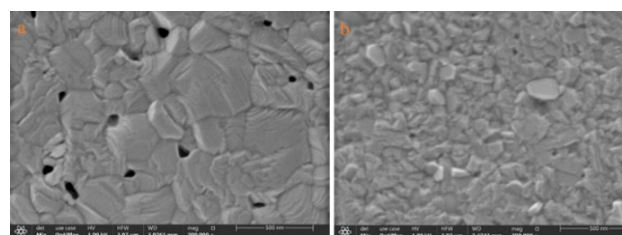


Figure 5. FESEM pictures of perovskite layers on (a) undoped and (b) Cu-doped CoO_x layers

Furthermore, the impact of Cu incorporation on CoO_x crystallinity was examined using X-ray diffraction. Figure 6 presents the XRD patterns of MAPbI_3 films deposited on pure and Cu-doped CoO_x substrates within the 2θ range of $10\text{--}80^\circ$. The X-ray maxima observed at 14.3° , 28.6° , and 32° correspond to the (110), (220), and (310) lattice planes, respectively [35]. Compared to the undoped CoO_x substrate, the perovskite thin film grown on the Cu-doped CoO_x layer displays a more intense and well-defined (110) diffraction peak, suggesting a notable enhancement in crystallinity. For pure and Cu-doped CoO_x , the (110) diffraction peak's full width at half maximum (FWHM) values were measured as 0.1 and 0.17, respectively. According to these results, the data indicates that the perovskite coated on Cu-doped CoO_x substrates has good crystallinity, which is beneficial to enhance the performance of perovskite solar cells [36-37].

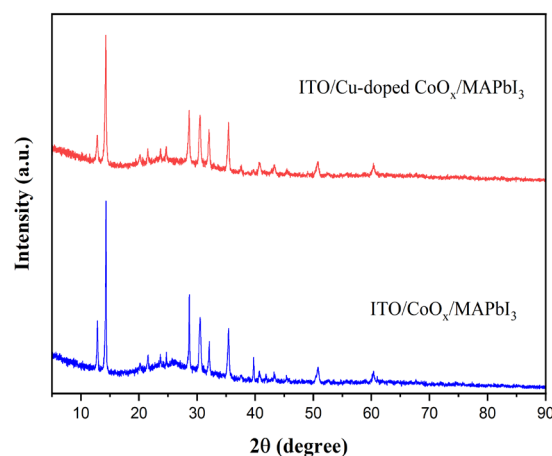


Figure 6. X-ray diffraction graphs of pure and Cu-doped CoO_x layers

The electrical characterization of the perovskite solar cells, both in dark and under illumination,

containing CoO_x and Cu-doped CoO_x HTLs, is given in Figure 7(a)-(b). The dark J-V graphs of the produced devices showed rectifying attributes. In comparison to the pure CoO_x -based device, the optimized device incorporating Cu as a dopant in the HTL exhibited significant enhancements in performance. The photovoltaic parameters of the fabricated cells are given in Table 1. The solar cell utilizing pure CoO_x achieved an open circuit voltage of 777 mV, a current density of 21.3 mA/cm^2 , a fill factor of 37.3%, and a power conversion efficiency (PCE)

of 6.17%. In contrast, the Cu-doped CoO_x -based device demonstrated an improved photovoltaic efficiency of 9%, having a V_{oc} of 862 mV, a J_{sc} of 24.3 mA/cm^2 , and a FF of 43.1% (Table 1). The enhanced photovoltaic performance can be explained by the better morphological characteristics of the CoO_x and perovskite layers, as well as the increased electrical conductivity facilitated by Cu doping.

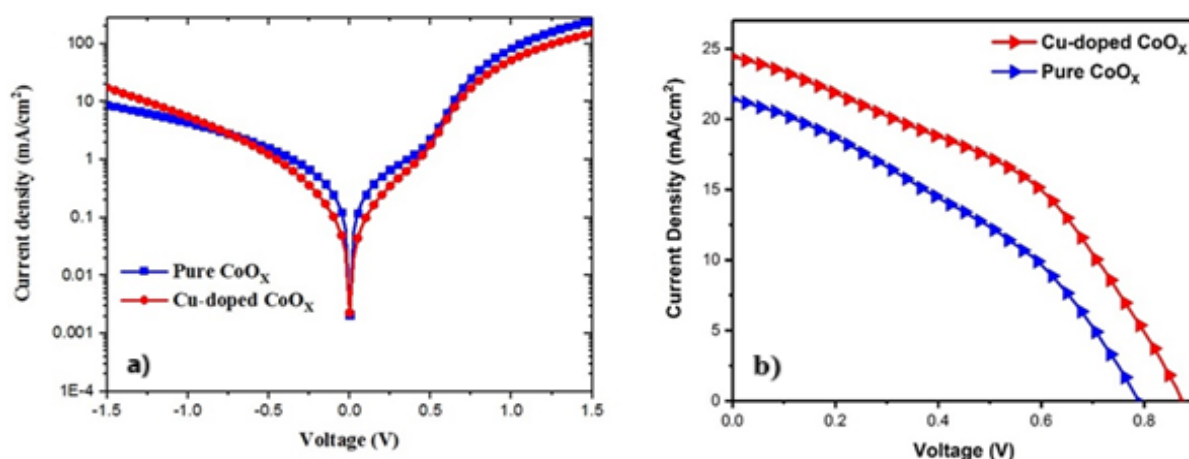


Figure 7. Current density-voltage curves for undoped and Cu-doped CoO_x hole transporting layer under (a) dark condition and (b) light condition

Table 1. Photovoltaic parameters of manufactured cells

Device	V_{oc} (mV)	J_{sc} (mA/cm^2)	FF (%)	PCE (%)	HF
Pure CoO_x	777	21.3	37.3	6.17	0.109
Cu-doped CoO_x	862	24.3	43.1	9.02	0.044

4. Conclusion

In summary, the influence of Cu doping on cobalt oxide layers in $(\text{CH}_3\text{NH}_3\text{PbI}_3)$ perovskite solar cells was investigated. AFM surface analysis demonstrated that the introduction of Cu into the cobalt oxide layer led to an increase in surface roughness. The introduction of a Cu-doped layer resulted in a perovskite active layer that was uniformly distributed and free from pinholes, as observed in the FE-SEM images. This modification also caused a decline in the grain boundaries and an increase in the size of the crystalline grains. As a consequence of these

enhancements, the V_{oc} , J_{sc} , and FF showed significant improvement, leading to a rise in perovskite solar cell efficiency from 6.17% to 9.02% with Cu incorporation. Therefore, Cu-doped cobalt oxide layers demonstrate strong potential as hole transport layer (HTL) candidates, requiring further investigation for their application in perovskite solar cells.

Article Information Form

The Declaration of Conflict of Interest/ Common Interest

No conflict of interest or common interest has been declared by the author.

Artificial Intelligence Statement

No artificial intelligence tools were used while writing this article.

Copyright Statement

The author owns the copyright of her work published in the journal and her work is published under the CC BY-NC 4.0 license.

References

- [1] J. Yan, B. Saunders, "Third-generation solar cells: A review and comparison of polymer: Fullerene, hybrid polymer and perovskite solar cells," *RSC Advances*, vol. 4, pp. 43286-43314, 2014.
- [2] A. Paulke, S. Stranks, J. Kniepert, J. Kurpiers, C. Wolff, N. Schön, H. Snaith, T. Brenner, D. Neher, "Charge carrier recombination dynamics in perovskite and polymer solar cells," *Applied Physics Letters*, vol. 108, 113505, 2016.
- [3] W. Li, Z. Wang, F. Deschler, S. Gao, R. Friend, A. Cheetham, "Chemically diverse and multifunctional hybrid organic-inorganic perovskites," *Nature Reviews Materials*, vol. 2, no. 3, pp. 1-18, 2017.
- [4] NREL Energy, "Best research cell Efficiency Chart," [Online]. Available: <http://www.nrel.gov/pv/cell-efficiency.html>
- [5] M. Green, "Third generation photovoltaics: Solar cells for 2020 and beyond," *Physica E: Low-Dimensional Systems and Nanostructures*, vol. 14, pp. 65-70, 2002.
- [6] J. Correa-Baena, M. Saliba, T. Buonassisi, M. Grätzel, A. Abate, W. Tress, A. Hagfeldt, "Promises and challenges of perovskite solar cells," *Science*, vol. 358, pp. 739-744, 2017.
- [7] R. Singh, V. Shukla, "ITIC-based bulk heterojunction perovskite film boosting the power conversion efficiency and stability of the perovskite solar cell," *Solar Energy*, vol. 178, pp. 90-97, 2019.
- [8] R. Singh, S. Sandhu, J. Lee, "Elucidating the effect of shunt losses on the performance of mesoporous perovskite solar cells," *Solar Energy*, vol. 193, pp. 956-961, 2019.
- [9] S. Mali, C. Hong, "P-i-n/n-i-p type planar hybrid structure of highly efficient perovskite solar cells towards improved air stability: Synthetic strategies and the role of p-type hole transport layer (HTL) and n-type electron transport layer (ETL) metal oxides," *Nanoscale*, vol. 8, no. 20, pp. 10528-10540, 2016.
- [10] Y. Yu, D. Zhao, C. Grice, W. Meng, C. Wang, W. Liao, A. Cimaroli, H. Zhang, K. Zhu, Y. Yan, "Thermally evaporated methylammonium tin triiodide thin films for lead-free perovskite solar cell fabrication," *RSC Advances*, vol. 6, pp. 90248-90254, 2016.
- [11] Q. Chen, H. Zhou, Z. Hong, S. Luo, H. Duan, H. Wang, Y. Liu, G. Li, Y. Yang, "Planar Heterojunction Perovskite Solar Cells via Vapor-Assisted Solution Process," *Journal of the American Chemical Society*, vol. 136, no. 2, pp. 622-625, 2014.
- [12] J. Pan, C. Mu, Q. Li, W. Li, D. Ma, D. Xu, "Room-Temperature, Hydrochloride-Assisted, One-Step Deposition for Highly Efficient and Air-Stable Perovskite Solar Cells," *Advanced Materials*, vol. 28, no. 37, pp. 8309-8314, 2016.
- [13] G. Wang, D. Liu, J. Xiang, D. Zhou, K. Alameh, B. Ding, Q. Song, "Efficient perovskite solar cell fabricated in ambient air using one-step spin-coating," *RSC Advances*, vol. 6, pp. 43299-43303, 2016.
- [14] S. Ulična, B. Dou, D. Kim, K. Zhu, J. Walls, J. Bowers, M. Van Hest, "Scalable deposition of high-efficiency perovskite solar cells by spray-coating," *ACS Applied Energy Materials*, vol. 1, no. 5, pp. 1853-1857, 2018.
- [15] F. Shao, L. Xu, Z. Tian, Y. Xie, Y. Wang, P. Sheng, D. Wang, F. Huang, "A modified two-step sequential deposition method for preparing perovskite $\text{CH}_3\text{NH}_3\text{PbI}_3$ solar cells," *RSC Advances*, vol. 6, pp. 42377-42381, 2016.

- [16] J. Liu, C. Gao, X. He, Q. Ye, L. Ouyang, D. Zhuang, C. Liao, J. Mei, W. Lau, "Improved crystallization of perovskite films by optimized solvent annealing for high efficiency solar cell," *ACS Applied Materials and Interfaces*, vol. 7, no. 43, pp. 24008-24015, 2015.
- [17] Z. Xiao, Q. Dong, C. Bi, Y. Shao, Y. Yuan, J. Huang, "Solvent Annealing of Perovskite-Induced Crystal Growth for Photovoltaic-Device Efficiency Enhancement," *Advanced Materials*, vol. 26, no. 37, pp. 6503-6509, 2014.
- [18] S. Paek, P. Schouwink, E. Athanasopoulou, K. Cho, G. Grancini, Y. Lee, Y. Zhang, F. Stellacci, M. Nazeeruddin, P. Gao, "From Nano- to Micrometer Scale: The Role of Antisolvent Treatment on High Performance Perovskite Solar Cells," *Chemistry of Materials*, vol. 29, no. 8, pp. 3490-3498, 2017.
- [19] J. Christians, J. Manser, P. Kamat, "Multifaceted excited state of $\text{CH}_3\text{NH}_3\text{PbI}_3$ charge separation, recombination, and trapping," *Journal of Physical Chemistry Letters*, vol. 6, pp. 2086-2095, 2015.
- [20] M. Mehrabian, E. Afshar, "Effect of different hole transport materials on photovoltaic properties in solar cells based on MAPbI_3 perovskite," *Bulletin of Materials Science*, vol. 44, no. 266, pp. 1-6, 2021.
- [21] X. Yin, Y. Guo, H. Xie, W. Que, L. Kong, "Nickel Oxide as Efficient Hole Transport Materials for Perovskite Solar Cells," *Solar RRL*, vol. 3, no. 5, pp. 1-27, 2019.
- [22] Z. Tseng, L. Chen, C. Chiang, S. Chang, C. Chen, C. Wu, "Efficient inverted-type perovskite solar cells using UV-ozone treated MoO_x and WO_x as hole transporting layers," *Solar Energy*, vol. 139, pp. 484-488, 2016.
- [23] H. Peng, W. Sun, Y. Li, S. Ye, H. Rao, W. Yan, H. Zhou, Z. Bian, C. Huang, "Solution processed inorganic V_2O_x as interfacial function materials for inverted planar-heterojunction perovskite solar cells with enhanced efficiency," *Nano Research*, vol. 9, pp. 2960-2971, 2016.
- [24] S. Chatterjee, A. Pal, "Introducing Cu_2O thin films as a hole-transport layer in efficient planar perovskite solar cell structures," *Journal of Physical Chemistry C*, vol. 120, no. 3, pp. 1428-1437, 2016.
- [25] A. Shalan, T. Oshikiri, S. Narra, M. Elshanawany, K. Ueno, H. Wu, K. Nakamura, X. Shi, E. Diau, H. Misawa, "Cobalt Oxide (CoO_x) as an Efficient Hole-Extracting Layer for High-Performance Inverted Planar Perovskite Solar Cells," *ACS Applied Materials and Interfaces*, vol. 8, no. 49, pp. 33592-33600, 2016.
- [26] F. Ma, Y. Zhao, J. Li, X. Zhang, H. Gu, J. You, "Nickel oxide for inverted structure perovskite solar cells," *Journal of Energy Chemistry*, vol. 49, pp. 393-411, 2021.
- [27] H. Alishah, "The influence of cadmium on the photovoltaic performance of CoO_x -based MAPbI_3 solar cells," *Applied Physics A: Materials Science and Processing*, vol. 130, no. 420, pp. 1-12, 2024.
- [28] A. Huang, L. Lei, Y. Yu, Y. Liu, S. Yang, S. Bao, X. Cao, P. Jin, "Enhanced electrical property of Ni-doped CoO_x hole transport layer for inverted perovskite solar cells," *Nanotechnology*, vol. 28, no. 20, pp. 1-7, 2017.
- [29] X. Wan, Y. Jiang, Z. Qiu, H. Zhang, X. Zhu, I. Sikandar, X. Liu, X. Chen, B. Cao, "Zinc as a new dopant for NiO_x -based planar perovskite solar cells with stable efficiency near 20%," *ACS Applied Energy Materials*, vol. 1, no. 8, pp. 3947-3954, 2018.

- [30] K. Yao, F. Li, Q. He, X. Wang, Y. Jiang, H. Huang, A. Jen, "A copper-doped nickel oxide bilayer for enhancing efficiency and stability of hysteresis-free inverted mesoporous perovskite solar cells," *Nano Energy*, vol. 40, pp. 155-162, 2017.
- [31] R. Kaneko, T. Chowdhury, G. Wu, E. Kayesh, S. Kazaoui, K. Sugawa, J. Lee, T. Noda, A. Islam, J. Otsuki, "Cobalt-doped nickel oxide nanoparticles as efficient hole transport materials for low-temperature processed perovskite solar cells," *Solar Energy*, vol. 181, pp. 243-250, 2019.
- [32] R. Islam, R. Abdur, A. Alam, N. Munna, A. Ahmed, M. Hossain, M. Bashir, D. Islam, M. Jamal, "Modulating Mn-doped NiO nanoparticles: Structural, optical, and electrical property tailoring for enhanced hole transport layers," *Nanoscale Advances*, vol. 7, pp. 133-143, 2025
- [33] K. Kim, C. Takahashi, Y. Abe, M. Kawamura, "Effects of Cu doping on nickel oxide thin film prepared by sol-gel solution process," *Optik*, vol. 125, no. 12, pp. 2899-2901, 2014.
- [34] Q. An, F. Paulus, D. Becker-Koch, C. Cho, Q. Sun, A. Weu, S. Bitton, N. Tessler, Y. Vaynzof, "Small grains as recombination hot spots in perovskite solar cells," *Matter*, vol. 4, pp. 1683-1701, 2021.
- [35] H. Alishah, "The performance of triethanolamine (TEOA)-doped Poly(3,4-ethylenedioxythiophene): Polystyrene sulfonate on MAPbI₃-based solar cells," *Optik*, vol. 311, pp. 1-12, 2024.
- [36] W. Kong, F. Zeng, Z. Su, T. Wang, L. Qiao, T. Ye, L. Zhang, R. Sun, J. Barbaud, F. Li, X. Gao, R. Zheng, X. Yang, "Oriented Low-n Ruddlesden-Popper Formamidinium-Based Perovskite for Efficient and Air Stable Solar Cells," *Advanced Energy Materials*, vol. 12, no. 46, pp. 1-10, 2022.
- [37] S. Cui, J. Wang, H. Xie, Y. Zhao, Z. Li, S. Luo, L. Ke, Y. Gao, K. Meng, L. Ding, Y. Yuan, "Rubidium ions enhanced crystallinity for ruddlesden–popper perovskites," *Advanced Science*, vol. 7, no. 24, 2002445, 2020.